Allergologia et immunopathologia
Sociedad Española de Inmunología Clínica, Alergología y Asma Pediátrica
www.all-imm.com

ORIGINAL ARTICLE

OPEN ACCESS

CHAC1 exacerbates LPS-induced ferroptosis and apoptosis in HK-2 cells by promoting oxidative stress

Zhihui Zhou[a], Hongwei Zhang[b]*

[a]*Department of Critical Care Medicine, Chongqing General Hospital, Chongqing, China*
[b]*Department of ICU, Affiliated Hospital of Hebei University, Baoding, Hebei, China*

Received 19 August 2022; Accepted 16 September 2022
Available online 1 March 2023

KEYWORDS
acute kidney injury;
apoptosis;
CHAC1;
ferroptosis;
oxidative stress

Abstract
Background: Sepsis-induced acute kidney injury (AKI) is a singularly grievous and life-threatening syndrome. Its pathogenesis is closely related to inflammatory response, apoptosis, oxidative stress, and ferroptosis. Cation transport regulator-like protein 1 (CHAC1), as a proapoptic factor, may be involved in apoptosis, oxidative stress, and ferroptosis. This study aimed to explore the role of CHAC1 in the lipopolysaccharide (LPS)-induced the human renal proximal tubular epithelial (HK-2) cells.
Methods: HK-2 cells were challenged with LPS to construct a model of sepsis-induced AKI *in vitro*. The role of CHAC1 in the LPS-induced HK-2 cells was explored using Western blot assay, cell counting kit-8 (CCK-8), flow cytometry, and colorimetric assays. Additionally, N-acetyl cysteine (NAC) was incubated with HK-2 cells to define deeply the relation between oxidative stress and apoptosis or ferroptosis.
Results: The expression of CHAC1 was enhanced in the kidney tissues of mice with sepsis-induced multiple organ dysfunction syndrome (MODS), through the Gene Expression Omnibus database (GSE60088 microarray dataset), and in the LPS-induced HK-2 cells. The cell viability was significantly reduced by LPS treatment, which was at least partly restored by the transfection of siCHAC1#1 and siCHAC1#2 but not siNC. In addition, down-regulation of CHAC1 counteracted the LPS-induced reactive oxygen species level and malonaldehyde concentrations while restored the LPS-induced glutathione concentrations. Meanwhile, interference of CHAC1 neutralized LPS-induced apoptosis rate, and the relative level of cleaved poly(ADP-ribose) polymerase (PARP)/PARP, and cleaved caspase-3/caspase-3. In addition, silencing of CHAC1 recovered the LPS-induced enhanced protein level of glutathione peroxidase 4 (GPx4) whereas antagonized the LPS-induced relative protein level of ACSL4 and that of iron. Moreover, application of NAC inverted the effect of CHAC1 on apoptosis and ferroptosis in HK-2 cells.
Conclusion: CHAC1 exacerbated ferroptosis and apoptosis by enhancing oxidative stress in LPS-induced HK-2 cells.

***Corresponding author:** Hongwei Zhang, Department of ICU, Affiliated Hospital of Hebei University, No. 212 East Road, Baoding, Hebei 071000, China. *Email address:* z_hongwei818@163.com

https://doi.org/10.15586/aei.v51i2.760

Introduction

Sepsis caused by infections of bacteria, fungi, or virus is an immensely severe and life-threatening syndrome. It leads to dysfunctioning of multiple organs and has been the leading cause of death in intensive care units (ICUs).[1,2] Acute kidney injury (AKI) is one of the most common and severe complications that emerges during the progression of sepsis, accounting for more than half of cases of AKI in Intensive care units.[3] Specifically, sepsis-induced AKI leads a six- to eight-fold increased risk of deaths among sepsis patients,[3,4] and also an increased incidence of progression of chronic kidney disease in sepsis survivors.[5] The development and progression of sepsis-induced AKI is an intricate crosstalk of multiple mechanisms, such as inflammatory response, oxidative stress, apoptosis, and ferroptosis.[6-9] Thus, despite advances in treatments, such as renal replacement, blood purification, and pharmacologic therapy,[10,11] high mortality and down-the-line outcomes still continue.[12] Therefore, exploring the potential molecular mechanisms of sepsis-induced AKI and seeking underlying targets could contribute to the development and improvement of therapies for sepsis-induced AKI.

Cation transport regulator-like protein 1 (CHAC1), situated in cytosol, has been identified in mammalian cells as a novel component of the unfolded protein response (UPR) pathway.[13] CHAC1 is under the modulation of the Activating Transcription Factor 4 (ATF4) arm, ATF3, and C/EBP homologous protein (CHOP), thus it is the downstream of ATF4–ATF3–CHOP pathway.[13] Notably, CHAC1 can promote apoptosis cascade via apoptosis-inducing factor (AIF) and poly(ADP-ribose) polymerase (PARP); so, it is generally recognized as a mammalian pro-apoptic factor.[13] In addition, CHAC1 can degrade glutathione (GSH) in the cytosol of mammalian cells through its gamma(γ)-glutamylcyclotransferase activity.[14] GSH is the most abundant non-protein thiol present in all mammalian tissues resistant to oxidative stress.[15] Moreover, depletion of GSH is demonstrated as an early hallmark of apoptosis.[16] Furthermore, GSH is the reducing substrate of glutathione peroxidase 4 (GPx4).[17] The insufficient activity or missing of GPx4 can lead to ferroptosis, indicating that GSH is also essential for ferroptosis.[17] In this study, we speculate that CHAC1 regulates the progress of sepsis-induced AKI through the modulation of apoptosis, oxidative stress, and ferroptosis.

In the current study, an *in vitro* model of sepsis-induced AKI was established in the human renal proximal tubular epithelial cells, HK-2 cells, with lipopolysaccharide (LPS) challenge. Then the role of CHAC1 in apoptosis, oxidative stress, and ferroptosis was investigated in LPS-induced HK-2 cells.

Materials and methods

Data extraction and analysis of differentially expressed genes (DEGs)

The GSE60088 microarray dataset was accessed from the Gene Expression Omnibus (GEO) database, which developed from the Affymetrix GPL1261 platform. It contained five lung cases of mice with sepsis-induced multiple organ dysfunction syndrome (MODS) challenged by a combination of mechanical ventilation and *S. aureus pneumonia* (MV+SA), four normal tissues from the lung, five liver cases of mice induced by MV+SA, three normal tissues from the liver, five kidney cases of mice induced by MV+SA (GSM1464844, GSM1464845, GSM1464846, GSM1464847, and GSM1464848), and five normal tissues from the kidney (GSM1464839, GSM1464840, GSM1464841, GSM1464842, and GSM1464843). The DEGs in kidney tissues and normal tissues were analyzed by using the LIMMA package in R language,[18] and the heat map, including the top 30 up-regulated and the top 30 down-regulated genes, was also imaged with the thresholds of logFC (fold change) of >1.0 and $P < 0.01$.

Functional enrichment identification

The functional enrichment identification was determined by the Metascape platform.[19] It integrated the analysis of GO biological processes, KEGG pathway, Reactome gene sets, CORUM, Wiki pathways, and PANTHER pathway20.

Cell culture

HK-2 cells (CL-0109) were acquired from Procell (Wuhan, China) and hatched in minimum essential medium (MEM, PM150410; Procell) with 10% fetal bovine serum (FBS, 164210-50; Procell) and 1% penicillin–streptomycin (PB180120; Procell) at 37°C in an incubator with 5% carbon dioxide (CO_2).

Cell treatment and transfection

In order to explore the optimal treatment time of LPS on HK-2 cells, cells were challenged with 10-μg/mL LPS (*Escherichia coli* 055:B5, L8880; Solarbio, Beijing, China) for 2, 4, 8, and 12 h.[20] Meanwhile, two small interfering (si) RNAs targeting CHAC1 (siCHAC1#1 and siCHAC1#2) and the corresponding negative control (siNC) were obtained from GenePharma (Shanghai, China) and transfected in HK-2 cells with lipofectamine 3000 (Invitrogen, Carlsbad, CA, USA) for 6 h. Then HK-2 cells were challenged with 10-μg/mL LPS for 8 h. In addition, to further verify the relation between oxidative stress and apoptosis or ferroptosis, HK-2 cells were transfected with plasmid cloning (pc)DNA vector plasmids harboring the sequences of CHAC1 (CHAC1) or the empty pcDNA vector plasmids (vector) with lipofectamine 3000; these were consecutively treated with 5-mM N-acetyl cysteine (NAC) for 1 h as well as 10-μg/mL LPS for 8 h.

Western blot analysis

As described by Fu et al.,[21] total proteins were extracted from cells with radioimmunoprecipitation assay (RIPA) buffer (R0010, Solarbio) and quantified with the bicinchoninic acid (BCA) protein assay kit (PC0020, Solarbio) by following the direction for use. Protein samples, 20 μg, were separated and electrically transferred onto a polyvinylidene fluoride (PVDF) membrane (EMD Millipore, Billerica, MA, USA). After sealing with 5% skimmed milk (Anchor, Switzerland) at room temperature for 1 h, the membranes were incubated overnight at 4°C with the following

primary antibodies targeted to diverse proteins: CHAC1 (1:500, ab217808; Abcam, Cambridge, UK), PARP (1:10,000, ab227244; Abcam), cleaved PARP (1:1000, ab4830; Abcam), caspase-3 (1:500, ab13847; Abcam), cleaved caspase-3 (1:100, ab2302; Abcam), GPx4 (1:1000, ab231174; Abcam), ACSL4 (1:10,000, 22401-1-AP; Proteintech, Wuhan, China) and β-actin (1:5000, ab8227; Abcam). The membranes were then hatched with goat anti-rabbit IgG H&L (HRP) (1:20,000; Abcam) at room temperature for 2 h and visualized by ECL Western blotting substrate (PE0010, Solarbio). The gray value was quantified by QUANTITY ONE software (Bio-Rad, Hercules, CA, USA).

Cell counting kit-8 (CCK-8) assay

The cell viability of HK-2 cells was assessed by CCK-8 assays (Dojindo Laboratories, Kumamoto, Japan) as described previously.[22] The optical density (OD) at 450 nm was detected by using a microplate reader (Thermo Fisher Scientific, Waltham, MA, USA).

Flow cytometry assay

The level of reactive oxygen species (ROS) in HK-2 cells was evaluated with the flow cytometry assay after cells were incubated with 5-(and-6)-chloromethyl-2',7'-dichlorofluorescin diacetate (CM-H2DCFH-DA) in the dark at 37°C for 30 min. For determining cell apoptosis, HK-2 cells were collected, rinsed with phosphate buffer saline (PBS) (P1010, Solarbio), resuspended by 0.5-mL bind buffer, and stained with 5-μL Annexin V/FITC (Thermo Fisher Scientific) and 5-μL propidium iodide (PI; Thermo Fisher Scientific) for 15 min at room temperature. Then, the relative fluorescence intensities and apoptosis of HK-2 cells were examined on a FACScan flow cytometer with the CellQuest software (BD Biosciences, NJ, USA).

Measurement of malonaldehyde (MDA) and GSH levels

The concentrations of MDA and GSH were detected with the MDA test kit (A003-1-1; Nanjing Jiancheng Bioengineering Institute, Nanjing, China) at 532 nm and the total glutathione/oxidized glutathione assay kit (A061-2-1; Nanjing Jiancheng Bioengineering Institute) at 405 nm according to the operating manual under a microplate reader (Thermo Fisher Scientific).

Iron examination

The level of iron was examined using an iron assay kit (MAK025; Sigma, St. Louis, MO, USA) following the operating instruction manual.

Statistical analysis

Results were expressed as mean ± standard deviation (SD). Data were examined by normal distribution, and the difference was tested with the Student's *t*-test between two groups or the one-way analysis of variance (ANOVA) between more than two groups, followed by *post hoc* Bonferroni test by the SPSS 26.0 software (IBM, Armonk, New York, USA). $P < 0.05$ was considered as statistically significant.

Results

CHAC1 was overexpressed in the kidneys of septic mice

Through the GEO database, 192 up-regulated genes and 78 down-regulated genes were identified in the mice with sepsis-induced MODS challenged by a combination of MV+SA (Supplementary Tables S1 and S2). The top 30 up-regulated and 30 down-regulated genes are listed in Figures 1A and 1B. Meanwhile, results in Figures 1A and 1C showed that the expression of CHAC1 was observably increased in the kidney tissues of mice induced with MV+SA with logFC = 3.568785 and FDR (P-value adjusted for multiple tests) = 2.65E-07, compared with the kidney tissues of normal mice. Moreover, the functional enrichment analysis of both 192 up-regulated and 78 down-regulated genes was executed through the Metascape platform. As displayed in Figures 1D and 1E, the up-regulated genes were mainly enriched in several pathways, including response to extracellular stimulus, positive regulation of cell death, regulation of DNA-templated transcription in response to stress, and apoptotic signaling pathway. The down-regulated genes were mainly enriched in metabolism of lipids, cholesterol biosynthesis, and glucose homeostasis.

Knockdown of CHAC1 reduced LPS-induced oxidative stress in HK-2 cells

In order to explore the role of CHAC1 in the sepsis-induced AKI, an *in vitro* model was established in HK-2 cells with LPS treatment. Following the exposure to LPS for 2, 4, 8, and 12 h, the level of CHAC1 was notably enhanced, with the CHAC1 expression being highest at 8 h of LPS challenge (Figure 2A). As the expression of CHAC1 was up-regulated in tissues of both kidneys of mice with sepsis-induced MODS and LPS-induced HK-2 cells, two siRNAs targeting CHAC1 (siCHAC1#1 and siCHAC1#2) were transfected into HK-2 cells to down-regulate the level of CHAC1 (Figure 2B). The cell viability was significantly reduced with LPS treatment, which was at least partly restored by the treatment of siCHAC1#1 and siCHAC1#2 but not siNC (Figure 2C). Additionally, treatment of siCHAC1#1 and siCHAC1#2 prominently decreased the LPS-induced ROS level and the MDA concentration, while opposite tendency was indicated in the GSH concentration (Figures 2D–F). Thus, the data indicated that silencing of CHAC1 attenuated LPS-induced oxidative stress in HK-2 cells.

Silencing of CHAC1 alleviated LPS-induced apoptosis in HK-2 cells

Furthermore, the apoptosis rate of HK-2 cells was prominently enhanced with LPS treatment, which was notably antagonized with the transfection of siCHAC1#2

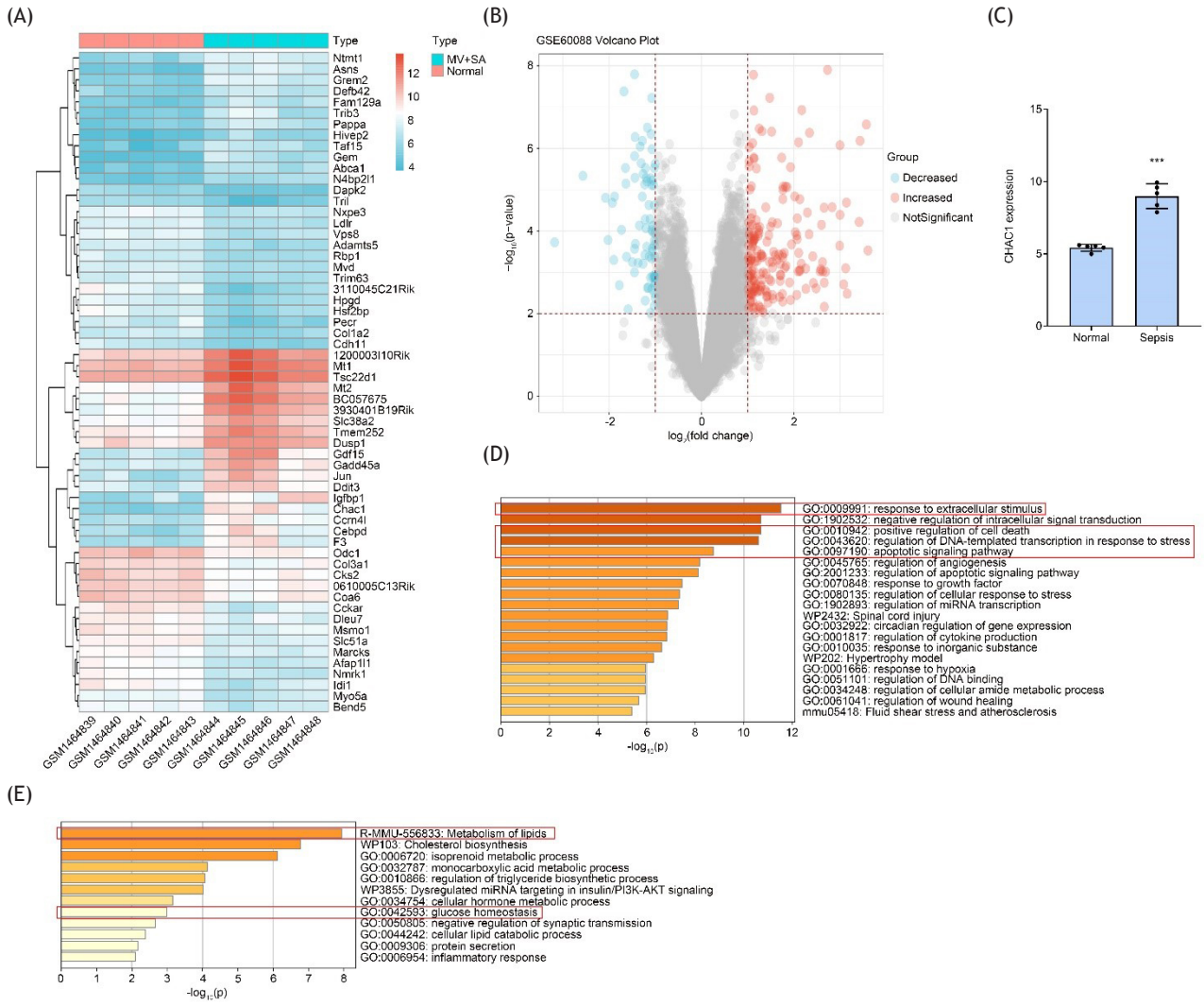

Figure 1 Analysis of core genes and functional enrichment about GSE60088. (A) The top 30 up-regulated and 30 down-regulated genes. (B) Volcanic plot of DEGs involved in the sepsis-induced multiple organ dysfunction syndrome (MODS) induced by a combination of MV+SA. (C) The expression level of CHAC1 was identified in the kidney tissues of mice induced with MV+SA, compared with that in the kidney tissues of normal mice. The biological process of (D) up-regulated and (E) down-regulated DEGs by functional enrichment analysis through Metascape platform.

(Figure 3A). Consistently, transfection of siCHAC1#2 significantly decreased the LPS-induced relative protein level of Cleaved PARP-PARP and cleaved caspase-3-caspase-3 (Figure 3B). Therefore, knockdown of CHAC1 relieved LPS-evoked apoptosis in HK-2 cells.

Interference of CHAC1 ameliorated LPS-induced ferroptosis in HK-2 cells

Moreover, the role of CHAC1 in ferroptosis was also dissected with knockdown of CHAC1 in HK-2 cells. Treatment of siCHAC1#2 observably increased the LPS-induced relative protein level of GPx4 whereas markedly reduced the LPS-induced relative level expression of ACSL4 (Figure 4A). In addition, administration of siCHAC1#2 significantly neutralized LPS-induced level of iron (Figure 4B). Hence, knockdown of CHAC1 improved LPS-induced ferroptosis in HK-2 cells.

CHAC1 exacerbated ferroptosis and apoptosis by promoting oxidative stress

In order to define relation between oxidative stress and apoptosis or ferroptosis, NAC, an antagonist of oxidative stress, was incubated with HK-2 cells. Transfection of CHAC1 overexpression plasmid markedly accelerated the reduction of the relative protein expression of GPx4 induced by LPS, which was notably improved with the application of NAC (Figure 5A). Meanwhile, an opposite result was observed in the relative protein expression of ACSL4 (Figure 5A). In addition, administration of NAC counteracted the up-regulation of CHAC1-induced MDA concentration, while it markedly recovered the up-regulation CHAC1-induced GSH concentration in LPS-treated HK-2 cells (Figure 5B). Moreover, co-transfection of CHAC1 overexpression plasmid prominently promoted both increased level of iron and rate of apoptosis induced by LPS, which

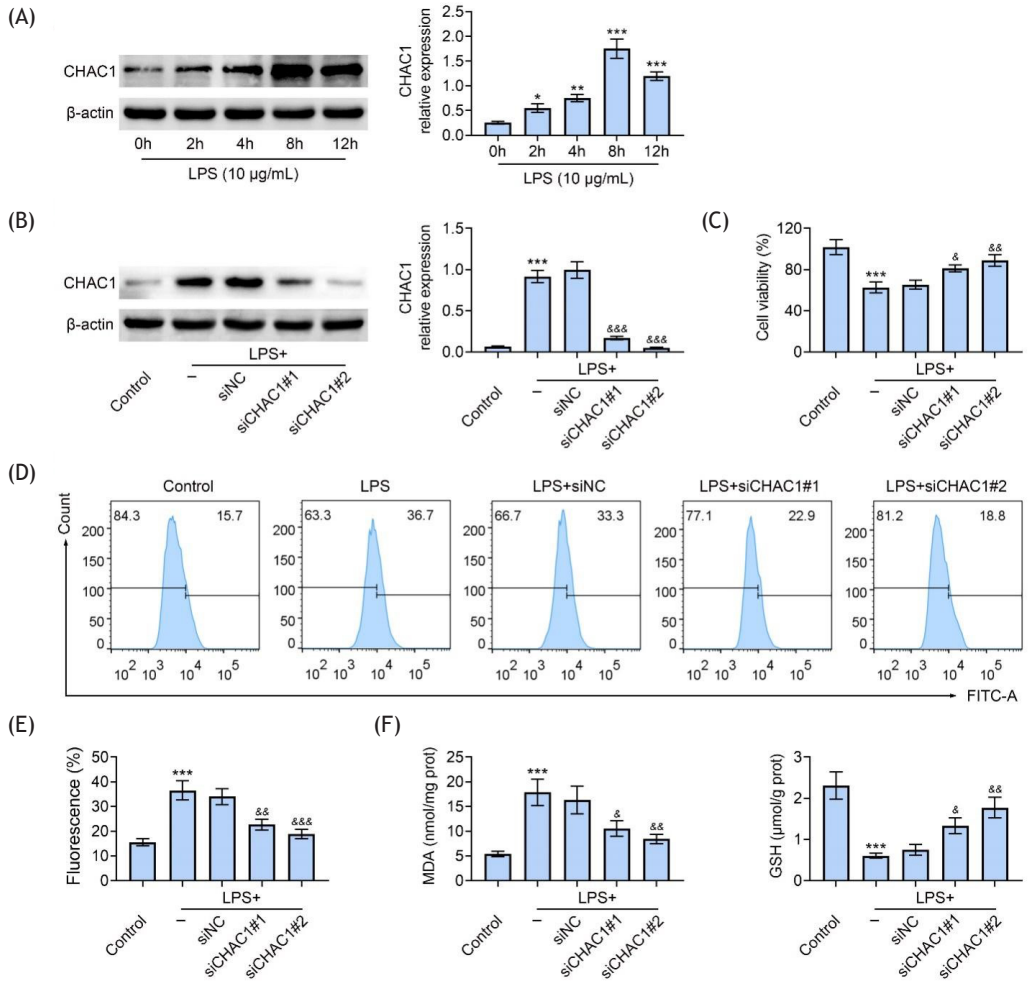

Figure 2 Down-regulation of CHAC1 declined LPS-induced levels of ROS, MDA, and GSH in HK-2 cells. The expression of CHAC1 was detected by Western blot analysis after HK-2 cells were (A) treated with 10-μg/mL LPS for 2, 4, 8, and 12 h, or (B) transfected with siCHAC1#1, siCHAC1#2, and the corresponding siNC. The data were expressed after normalized with β-actin. (C) The cell viability of HK-2 cells was examined by CCK-8 assays. (D and E) The ROS level of HK-2 cells was determined by flow cytometry. (F) The concentrations of MDA and GSH were measured with commercial kits. (A) *P < 0.05, **P < 0.01, and ***P < 0.001 vs. 0 h. (B–F) ***P < 0.001 vs. control; and &P < 0.05, &&P < 0.01, and &&&P < 0.001 vs. LPS.

were observably reversed with the use of NAC (Figures 5C and D). Taken together, CHAC1 aggravated ferroptosis and apoptosis by enhancing oxidative stress in LPS-induced HK-2 cells.

Discussion

Sepsis-induced AKI is a singularly grievous complication during the progression of sepsis, which has caused tremendous load on both patients and the society.[3,4] It has been demonstrated that the pathogenesis of sepsis-induced AKI is closely associated with inflammatory response, apoptosis, oxidative stress, and ferroptosis.[6-8] CHAC1 is identified as a mammalian pro-apoptotic factor,[13] which may be involved in apoptosis, oxidative stress, and ferroptosis. In the present study, the level of CHAC1 was found to be up-regulated in the kidney tissues of mice with sepsis-induced MODS according to bioinformatic analysis. The HK-2 cells were challenged with LPS to construct an *in vitro* model of sepsis-induced AKI. The CHAC1 level was consistently up-regulated in the LPS-induced HK-2 cells. Knockdown of CHAC1 dampened LPS-induced oxidative stress, apoptosis, and ferroptosis in HK-2 cells. Moreover, the application of NAC reversed the effects of CHAC1 on the apoptosis and ferroptosis of LPS-induced HK-2 cells. Taken together, CHAC1 aggravated LPS-induced ferroptosis and apoptosis in HK-2 cells by promoting oxidative stress.

CHAC1 is a novel component of UPR pathway, whose dysregulation has been reported in a variety of disease models. For instance, upregulation of CHAC1 has been discovered in intraocular (uveal tract) melanoma patients, predicting a poor outcome.[23] Similar results are also reported in breast and ovarian cancer patients.[24] In line with these findings, we also found that the expression of CHAC1 was enhanced in the kidney tissues of mice with sepsis-induced MODS based on bioinformatic analysis. Moreover, the CHAC1 was consistently expressed highly in LPS-induced HK-2 cells. Therefore, CHAC1 was overexpressed in sepsis-induced AKI.

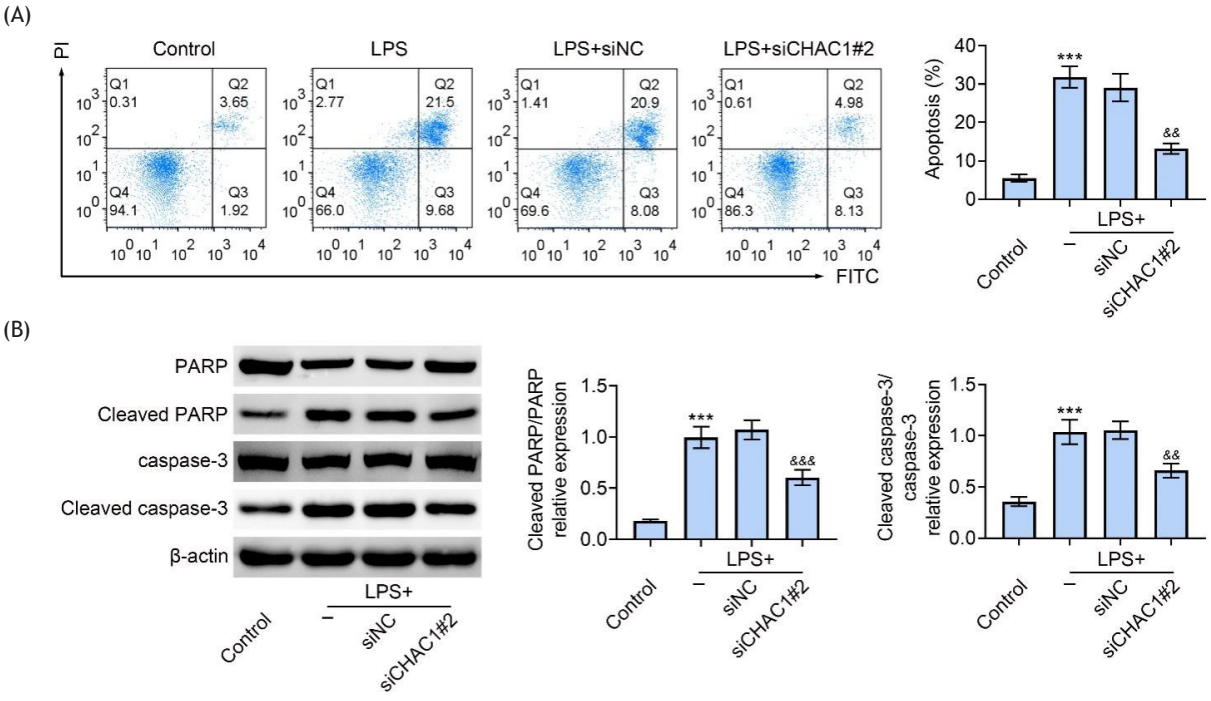

Figure 3 Knockdown of CHAC1-mitigated LPS-induced apoptosis in HK-2 cells. (A) The apoptosis rate of HK-2 cells was examined by flow cytometry. (B) The relative protein expressions of cleaved PARP–PARP and cleaved caspase-3–caspase-3 were determined by Western blot analysis. The data were expressed after normalized with β-actin. ***P < 0.001 vs. control; &&P < 0.01, and &&&P < 0.001 vs. LPS.

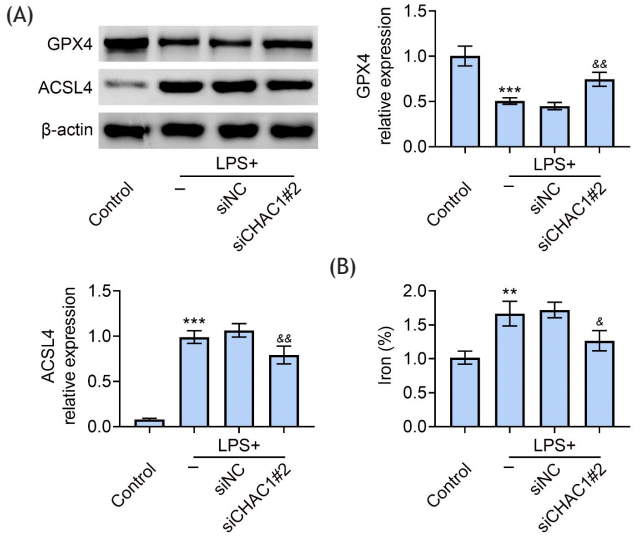

Figure 4 Silencing of CHAC1-mitigated LPS-induced ferroptosis in HK-2 cells. (A) The relative protein expressions of GPx4 and ACSL4 were determined by Western blot analysis. The data were expressed after normalized with β-actin. (B) The level of iron was measured with an iron assay kit. **P < 0.01 and ***P < 0.001 vs. control; &P < 0.05 and &&P < 0.01 vs. LPS.

Molecular mechanisms, such as apoptosis, oxidative stress, and ferroptosis, have been revealed to participate in the progression of a variety of diseases.[25-30] In sepsis-induced AKI, Huang et al. demonstrated that suppressing pannexin-1 inhibited cell apoptosis, which could contribute to the remission of sepsis-induced AKI.[31] Methyl jasmonate, a bioactive oxylipid, attenuates apoptosis and inflammation in LPS-induced HK-2 cells.[32] Similarly, surfactant protein D, an innate immune molecule, mitigates sepsis-induced AKI by reducing apoptosis.[33] Ibrutinib, an inhibitor of Bruton's tyrosine kinase, attenuates oxidative stress in the kidney of AKI-associated dysfunction.[34] Al-Harbi et al. reported that spleen tyrosine kinase signaling relieves sepsis-induced AKI by inhibiting inflammation and oxidative stress.[35] In addition, the study conducted by Guo et al. revealed that ginsenoside Rg1, belonging to the class of steroid glycosides, suppressed ferroptosis to improve sepsis-induced AKI.[6] Moreover, ferroptosis was involved in LPS-induced AKI through mitochondria-derived ROS.[36] In this study, our results also demonstrated that LPS treatment enhanced cell apoptosis, oxidative stress, and ferroptosis in HK-2 cells that were notably attenuated by the knockdown of CHAC1. CHAC1 acts as a proapoptotic factor,[13] and promotes apoptosis in temozolomide-induced glioma cytotoxicity.[37] More importantly, CHAC1 mediates the degradation of GSH,[14] which is strongly related to oxidative stress,[15] apoptosis,[16] and ferroptosis.[17] Taken together, these results demonstrated that silencing of CHAC1 attenuated LPS-induced oxidative stress, apoptosis, and ferroptosis in HK-2 cells.

Owing to harmful stimulation of external and internal conditions, oxidative stress generates superfluous ROS, which can assault cell DNA, protein, and lipid, eventually resulting in a series of pathogenies, such as apoptosis and ferroptosis.[38,39] Cui et al. showed that alfalfa saponins, a natural extract of Alfalfa (*Medicago sativa*), suppressed oxidative stress-mediated apoptosis in piglet cells.[40]

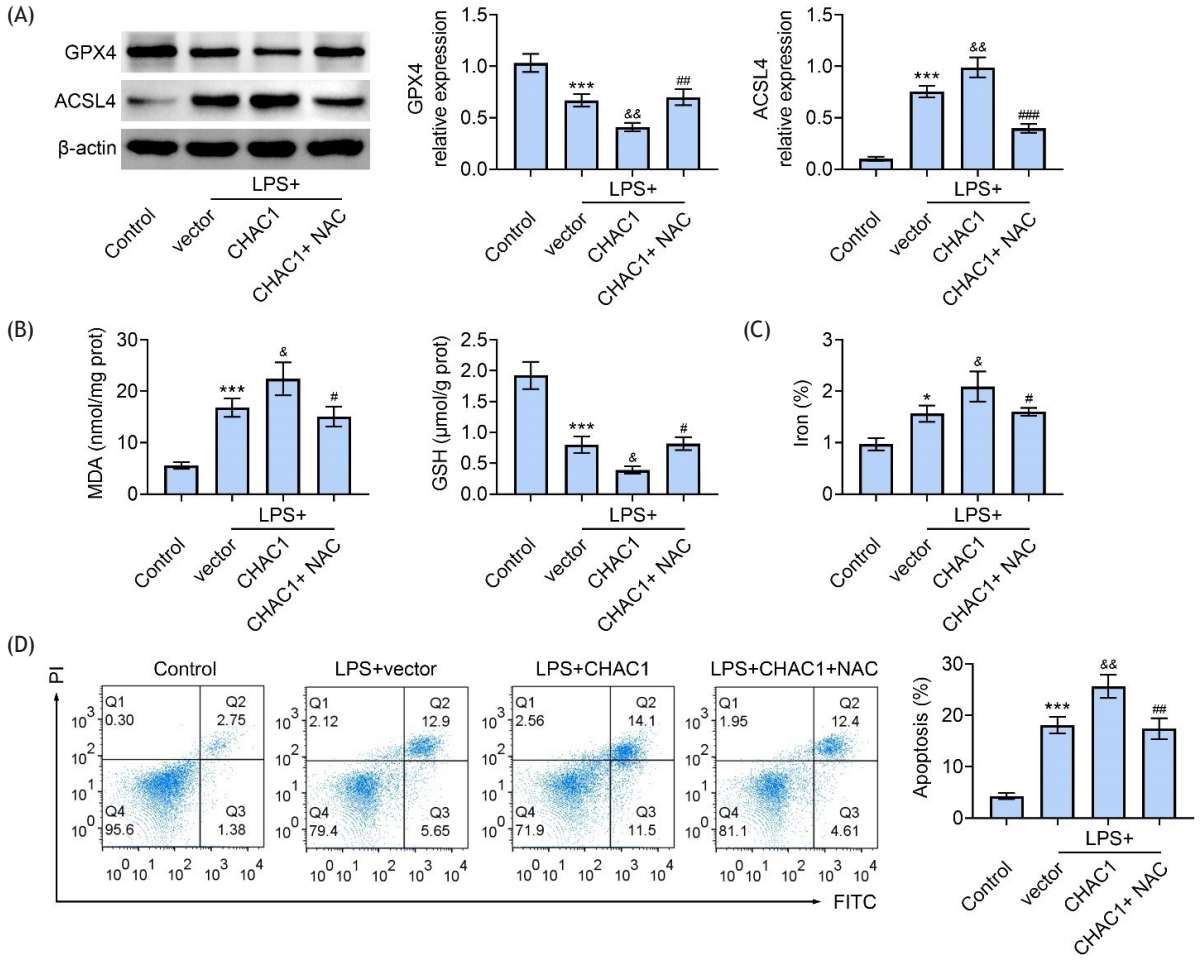

Figure 5 CHAC1 promoted ferroptosis and apoptosis by accelerating oxidative stress in LPS-induced HK-2 cells. (A) The relative protein expressions of GPx4 and ACSL4 were determined by Western blot analysis. The data were expressed after normalized with β-actin. (B) The concentrations of MDA and GSH were measured with commercial kits. (C) The level of iron was measured with an iron assay kit. (D) The apoptosis rate of HK-2 cells was examined by flow cytometry. *$P < 0.05$ and ***$P < 0.001$ vs. control; $^{\&}P < 0.05$ and $^{\&\&}P < 0.01$ vs. LPS+vector; $^{\#}P < 0.05$, $^{\#\#}P < 0.01$, and $^{\#\#\#}P < 0.001$ vs. LPS+CHAC1.

Bardoxolone methyl, a semi-synthetic triterpenoid, mitigates osteoarthritis by preventing oxidative stress-induced apoptosis.[41] Similarly, Zhu et al. summarized the molecular mechanisms of modulating oxidative stress-induced ferroptosis, and its potential therapeutic value in cancer.[28] In addition, oxidative stress-induced ferroptosis is also involved in the progression of intervertebral disc degeneration.[42] Similar these previous findings, NAC, an inhibitor of oxidative stress, reversed the effect of CHAC1 on apoptosis and ferroptosis in LPS-induced HK-2 cells in the current study, indicating that the role of CHAC1 in the pathogenies of LPS-induced HK-2 cells was associated with oxidative stress-induced apoptosis and ferroptosis.

Conclusion

The expression of CHAC1 was up-regulated in the kidney tissues of mice with sepsis-induced MODS and LPS-induced HK-2 cells. Overexpression of CHAC1 promoted the apoptosis, oxidative stress, and ferroptosis of LPS-induced HK-2 cells. Furthermore, the application of NAC reversed the effects of CHAC1 on the apoptosis and ferroptosis of LPS-induced HK-2 cells. Taken together, these findings illustrated that CHAC1 exacerbated ferroptosis and apoptosis by enhancing oxidative stress in LPS-induced HK-2 cells. However, an *in vivo* validation is essential in the present study. In brief, our study contributes to understand the molecular mechanisms for sepsis-induced AKI, which could further provide a potential target for AKI therapy.

Availability of Data and Materials

All data generated or analyzed during this study are included in this published article.

Competing interests

The authors stated that there were no conflicts of interest to disclose.

Author Contributions

Both authors contributed to conception and designing of the study. Material preparation and experiments were performed by Zhihui Zhou. Data collection and analysis were performed by both authors. The first draft of the manuscript was prepared by Hongwei Zhang. Both authors commented on the previous versions of the manuscript, and read and approved the final manuscript.

References

1. Salomão R, Ferreira BL, Salomão MC, Santos SS, Azevedo LCP, Brunialti MKC. Sepsis: Evolving concepts and challenges. Braz J Med Biol Res. 2019;52:e8595. https://doi.org/10.1590/1414-431x20198595
2. Liang W, Guo L, Liu T, Qin S. MEF2C alleviates acute lung injury in cecal ligation and puncture (CLP)-induced sepsis rats by up-regulating AQP1. Allergol Immunopathol (Madr). 2021;49:117-24. https://doi.org/10.15586/aei.v49i5.477
3. Uchino S, Kellum JA, Bellomo R, Doig GS, Morimatsu H, Morgera S, et al. Acute renal failure in critically ill patients: A multinational, multicenter study. JAMA. 2005;294:813-8. https://doi.org/10.1001/jama.294.7.813
4. Thakar CV, Christianson A, Freyberg R, Almenoff P, Render ML. Incidence and outcomes of acute kidney injury in intensive care units: A veterans administration study. Crit Care Med. 2009;37:2552-8. https://doi.org/10.1097/CCM.0b013e3181a5906f
5. Murugan R, Kellum JA. Acute kidney injury: What's the prognosis? Nat Rev Nephrol. 2011;7:209-17. https://doi.org/10.1038/nrneph.2011.13
6. Guo J, Wang R, Min F. Ginsenoside Rg1 ameliorates sepsis-induced acute kidney injury by inhibiting ferroptosis in renal tubular epithelial cells. J Leukoc Biol. 2022;112(5):1065-77. https://doi.org/10.1002/JLB.1A0422-211R
7. Chen Y, Jin S, Teng X, Hu Z, Zhang Z, Qiu X, et al. Hydrogen sulfide attenuates LPS-induced acute kidney injury by inhibiting inflammation and oxidative stress. Oxid Med Cell Longev. 2018;2018:6717212. https://doi.org/10.1155/2018/6717212
8. Wang Z, Wu J, Hu Z, Luo C, Wang P, Zhang Y, et al. Dexmedetomidine alleviates lipopolysaccharide-induced acute kidney injury by inhibiting p75NTR-mediated oxidative stress and apoptosis. Oxid Med Cell Longev. 2020;2020:5454210. https://doi.org/10.1155/2020/5454210
9. Song C, Adili A, Kari A, Abuduhaer A. FSTL1 aggravates sepsis-induced acute kidney injury through regulating TLR4/MyD88/NF-κB pathway in newborn rats. Signa Vitae. 2021;17:167-73.
10. Evans L, Rhodes A, Alhazzani W, Antonelli M, Coopersmith CM, French C, et al. Surviving sepsis campaign: International guidelines for management of sepsis and septic shock 2021. Intensive Care Med. 2021;47:1181-247. https://doi.org/10.1007/s00134-021-06506-y
11. Keir I, Kellum JA. Acute kidney injury in severe sepsis: Pathophysiology, diagnosis, and treatment recommendations. J Vet Emerg Crit Care (San Antonio). 2015;25:200-9. https://doi.org/10.1111/vec.12297
12. Peerapornratana S, Manrique-Caballero CL, Gómez H, Kellum JA. Acute kidney injury from sepsis: Current concepts, epidemiology, pathophysiology, prevention and treatment. Kidney Int. 2019;96:1083-99. https://doi.org/10.1016/j.kint.2019.05.026
13. Mungrue IN, Pagnon J, Kohannim O, Gargalovic PS, Lusis AJ. CHAC1/MGC4504 is a novel proapoptotic component of the unfolded protein response, downstream of the ATF4-ATF3-CHOP cascade. J Immunol. 2009;182:466-76. https://doi.org/10.4049/jimmunol.182.1.466
14. Kumar A, Tikoo S, Maity S, Sengupta S, Sengupta S, Kaur A, et al. Mammalian proapoptotic factor ChaC1 and its homologues function as γ-glutamyl cyclotransferases acting specifically on glutathione. EMBO Rep. 2012;13:1095-101. https://doi.org/10.1038/embor.2012.156
15. Lu SC. Glutathione synthesis. Biochim Biophys Acta. 2013;1830:3143-53. https://doi.org/10.1016/j.bbagen.2012.09.008
16. Circu ML, Aw TY. Glutathione and apoptosis. Free Radic Res. 2008;42:689-706. https://doi.org/10.1080/10715760802317663
17. Ursini F, Maiorino M. Lipid peroxidation and ferroptosis: The role of GSH and GPx4. Free Radic Biol Med. 2020;152:175-85. https://doi.org/10.1016/j.freeradbiomed.2020.02.027
18. Smyth GK. Linear models and empirical bayes methods for assessing differential expression in microarray experiments. Stat Appl Genet Mol Biol. 2004;3:Article 3. https://doi.org/10.2202/1544-6115.1027
19. Zhou Y, Zhou B, Pache L, Chang M, Khodabakhshi AH, Tanaseichuk O, et al. Metascape provides a biologist-oriented resource for the analysis of systems-level datasets. Nat Commun. 2019;10:1523. https://doi.org/10.1038/s41467-019-09234-6
20. Deng Z, Sun M, Wu J, Fang H, Cai S, An S, et al. SIRT1 attenuates sepsis-induced acute kidney injury via Beclin1 deacetylation-mediated autophagy activation. Cell Death Dis. 2021;12:217. https://doi.org/10.1038/s41419-021-03508-y
21. Fu Y, Jin R-R, Li Y-L, Luan H, Huang T, Zhao Y, et al. Isocorydine inhibits the proliferation of human endometrial carcinoma HEC-1B cells by downregulating the Ras/MEK/ERK signaling pathway. EJGO. 2021;42:548-53. https://doi.org/10.31083/j.ejgo.2021.03.5225
22. Chhabra R, Rao S, Kumar BM, Shetty AV, Hegde AM, Bhandary M. Characterization of stem cells from human exfoliated deciduous anterior teeth with varying levels of root resorption. J Clin Pediatr Dent. 2021;45:104-11. https://doi.org/10.17796/1053-4625-45.2.6
23. Liu Y, Li M, Shi D, Zhu Y. Higher expression of cation transport regulator-like protein 1 (CHAC1) predicts of poor outcomes in uveal melanoma (UM) patients. Int Ophthalmol. 2019;39:2825-32. https://doi.org/10.1007/s10792-019-01129-1
24. Goebel G, Berger R, Strasak AM, Egle D, Müller-Holzner E, Schmidt S, et al. Elevated mRNA expression of CHAC1 splicing variants is associated with poor outcome for breast and ovarian cancer patients. Br J Cancer. 2012;106:189-98. https://doi.org/10.1038/bjc.2011.510
25. Gui Y, Sun L, Liu R, Luo J. Pachymic acid inhibits inflammation and cell apoptosis in lipopolysaccharide (LPS)-induced rat model with pneumonia by regulating NF-κB and MAPK pathways. Allergol Immunopathol (Madr). 2021;49:87-93. https://doi.org/10.15586/aei.v49i5.468
26. Pritam P, Manna S, Sahu A, Swain SS, Ramchandani S, Bissoyi S, et al. Eosinophil: A central player in modulating pathological complexity in asthma. Allergol Immunopathol (Madr). 2021;49:191-207. https://doi.org/10.15586/aei.v49i2.50
27. Zhu F, Yu Z, Li D. miR-187 Modulates cardiomyocyte apoptosis and oxidative stress in myocardial infarction mice via negatively regulating DYRK2. Signa Vitae. 2021;17:142-50. https://doi.org/10.21203/rs.3.rs-291355/v1
28. Zhu J, Xiong Y, Zhang Y, Wen J, Cai N, Cheng K, et al. The molecular mechanisms of regulating oxidative stress-induced ferroptosis and therapeutic strategy in tumors. Oxid Med Cell Longev. 2020;2020:8810785. https://doi.org/10.1155/2020/8810785
29. Jin Y, Sun L, Liu K-C. Effect of sufentanil on the viability and apoptosis of cervical cancer cells via the inactivation

of PI3K/AKT/mTOR signaling pathway. Eur J Gynaecol Oncol. 2021;42:325–32. https://doi.org/10.31083/j.ejgo.2021.02.2257
30. Qian D, Zhu Y, Xu L, Dong T, Chen T, Yu Z. Icariin induces apoptosis in breast cancer MCF-7 cells by regulating the MELK-mediated PI3K/AKT signaling pathway. Eur J Gynaecol Oncol. 2021;42:957–65. https://doi.org/10.31083/j.ejgo4205144
31. Huang G, Bao J, Shao X, Zhou W, Wu B, Ni Z, et al. Inhibiting pannexin-1 alleviates sepsis-induced acute kidney injury via decreasing NLRP3 inflammasome activation and cell apoptosis. Life Sci. 2020;254:117791. https://doi.org/10.1016/j.lfs.2020.117791
32. Chen F, Wang W, Cai X, Yu H, Qu C, Zhang X, et al. Methyl jasmonate reduces the inflammation and apoptosis of HK-2 cells induced by LPS by regulating the NF-κB pathway. Signa Vitae. 2021;17:218–24.
33. Lu SJ, Xu JH, He ZF, Wu P, Ning C, Li HY. Innate immune molecule surfactant protein D attenuates sepsis-induced acute kidney injury through modulating apoptosis and NFκB-mediated inflammation. Int Wound J. 2020;17:100–06. https://doi.org/10.1111/iwj.13237
34. Nadeem A, Ahmad SF, Al-Harbi NO, Ibrahim KE, Alqahtani F, Alanazi WA, et al. Bruton's tyrosine kinase inhibition attenuates oxidative stress in systemic immune cells and renal compartment during sepsis-induced acute kidney injury in mice. Int Immunopharmacol. 2021;90:107123. https://doi.org/10.1016/j.intimp.2020.107123
35. Al-Harbi NO, Nadeem A, Ahmad SF, Alanazi MM, Aldossari AA, Alasmari F. Amelioration of sepsis-induced acute kidney injury through inhibition of inflammatory cytokines and oxidative stress in dendritic cells and neutrophils respectively in mice: Role of spleen tyrosine kinase signaling. Biochimie. 2019;158:102–10. https://doi.org/10.1016/j.biochi.2018.12.014
36. Liang NN, Zhao Y, Guo YY, Zhang ZH, Gao L, Yu DX, et al. Mitochondria-derived reactive oxygen species are involved in renal cell ferroptosis during lipopolysaccharide-induced acute kidney injury. Int Immunopharmacol. 2022;107:108687. https://doi.org/10.1016/j.intimp.2022.108687
37. Chen PH, Shen WL, Shih CM, Ho KH, Cheng CH, Lin CW, et al. The CHAC1-inhibited Notch3 pathway is involved in temozolomide-induced glioma cytotoxicity. Neuropharmacology. 2017;116:300–14. https://doi.org/10.1016/j.neuropharm.2016.12.011
38. Duan X, Wen Z, Shen H, Shen M, Chen G. Intracerebral hemorrhage, oxidative stress, and antioxidant therapy. Oxid Med Cell Longev. 2016;2016:1203285. https://doi.org/10.1155/2016/1203285
39. Yu Y, Yan Y, Niu F, Wang Y, Chen X, Su G, et al. Ferroptosis: A cell death connecting oxidative stress, inflammation and cardiovascular diseases. Cell Death Discov. 2021;7:193. https://doi.org/10.1038/s41420-021-00579-w
40. Cui Y, Li F, Zhu X, Xu J, Muhammad A, Chen Y, et al. Alfalfa saponins inhibit oxidative stress-induced cell apoptosis through the MAPK signaling pathway. Redox Rep. 2022;27:1–8. https://doi.org/10.1080/13510002.2021.2017681
41. Pang Z, Jiang Z, Zhu R, Song C, Tang H, Cao L, et al. Bardoxolone-methyl prevents oxidative stress-mediated apoptosis and extracellular matrix degradation in vitro and alleviates osteoarthritis in vivo. Drug Des Devel Ther. 2021;15:3735–47. https://doi.org/10.2147/DDDT.S314767
42. Lu S, Song Y, Luo R, Li S, Li G, Wang K, et al. Ferroportin-dependent iron homeostasis protects against oxidative stress-induced nucleus pulposus cell ferroptosis and ameliorates intervertebral disc degeneration in vivo. Oxid Med Cell Longev. 2021;2021:6670497. https://doi.org/10.1155/2021/6670497

Supplementary

Table S1 192 up-regulated genes identified in the mice with sepsis-induced multiple organ dysfunction syndrome (MODS) challenged by a combination of MV+SA through the GEO database.

Genes	logFC	FDR	Increased/ Decreased
Asns	2.7287764	1.25E-08	Increased
Aqp2	1.1250556	1.64E-08	Increased
Mthfd2	1.477257	5.97E-08	Increased
Grem2	2.1696646	1.18E-07	Increased
Pde3b	1.1349672	1.21E-07	Increased
Chac1	3.568785	2.65E-07	Increased
Ankrd44	1.2494606	3.36E-07	Increased
Eif4ebp1	1.3095008	3.83E-07	Increased
N4bp2l1	1.5183226	3.92E-07	Increased
Gem	2.338981	4.22E-07	Increased
BC057675	3.432074	6.54E-07	Increased
Ccrn4l	2.1009266	7.13E-07	Increased
Impact	1.1077478	7.46E-07	Increased
3930401B19Rik	2.998726	8.42E-07	Increased
Epc2	1.0347294	9.31E-07	Increased
Lox	1.1324036	1.68E-06	Increased
Abca1	1.7352976	1.68E-06	Increased
Slc4a7	1.1404486	1.78E-06	Increased
Iars	1.0323458	2.04E-06	Increased
Crebrf	1.0356382	2.71E-06	Increased
Pappa	1.927339	2.84E-06	Increased
LOC102641248	1.1901196	3.05E-06	Increased
Samd4	1.082359	8.33E-06	Increased
Fam129a	1.8203192	8.45E-06	Increased
Ntmt1	1.767826	8.46E-06	Increased
Dusp1	1.8535356	8.65E-06	Increased
Herpud1	1.0497682	9.83E-06	Increased
Hivep2	1.7611584	1.00E-05	Increased
Slc38a2	2.018034	1.46E-05	Increased
Mt1	1.7616932	1.69E-05	Increased
Tmem252	2.1276938	1.70E-05	Increased
Jun	3.138722	2.05E-05	Increased
Mt2	2.8267536	2.66E-05	Increased
Acot1	1.3914928	2.67E-05	Increased
Gadd45a	2.6541128	2.73E-05	Increased
Ddit3	2.2931718	3.59E-05	Increased
Bmp6	1.1014484	3.75E-05	Increased
Igfbp1	2.9998852	4.05E-05	Increased
1200003I10Rik	2.0742244	4.93E-05	Increased
Rsf1	1.0732624	5.02E-05	Increased
Sik3	1.1873406	5.49E-05	Increased
Gdf15	3.4121128	6.08E-05	Increased
Defb42	1.5317554	6.14E-05	Increased
Pknox1	1.014099	6.17E-05	Increased
Tsc22d1	1.6451374	6.49E-05	Increased
Cebpd	2.5979444	7.10E-05	Increased
Heca	1.1014634	7.19E-05	Increased
Acot2	1.4940364	7.87E-05	Increased
Cxcr4	1.263346	8.05E-05	Increased
4833417J20Rik	1.0451108	8.07E-05	Increased
Wsb1	1.2036194	8.35E-05	Increased
Acot1	1.2403522	9.67E-05	Increased
Slc10a6	1.0297598	0.000106911	Increased
Trib3	2.0300574	0.000107329	Increased
Sirt1	1.245763	0.000112285	Increased
F3	2.3296726	0.000120095	Increased
Tmem140	1.0298026	0.00012365	Increased
Bhlhe40	1.4578478	0.000126589	Increased
Taf15	2.065017	0.000127136	Increased
Klf4	1.138702	0.000130674	Increased
Snhg12	1.227534	0.000131197	Increased
Slc25a30	1.1044906	0.000132551	Increased
Sowahb	1.0507164	0.000141701	Increased
Slc25a25	1.1656498	0.000142668	Increased
Med13l	1.1541654	0.000154594	Increased
Nr4a1	2.069733	0.000158245	Increased
Ago2	1.0669838	0.000159114	Increased
Ncl	1.1364296	0.00016705	Increased
Clk4	1.1363582	0.000167724	Increased
Psap	1.1172824	0.000180131	Increased
Ppp1r15a	1.4149256	0.000181969	Increased
Bach2	1.100139	0.000198691	Increased
Ier3	1.9481224	0.000211141	Increased
Ino80d	1.0164334	0.00022642	Increased
Plk3	2.99106	0.000227415	Increased
Gp49a	1.1075492	0.000231396	Increased
Kctd15	1.0742292	0.000288198	Increased
Pdk4	3.6035404	0.000296854	Increased
Hipk3	1.2016954	0.000302348	Increased
Nop58	1.561047	0.000321979	Increased
Ch25h	2.1043216	0.000338813	Increased
Pald1	1.7935816	0.000339677	Increased
Eif4a1	1.292454	0.000368958	Increased
Osmr	1.6761746	0.000370069	Increased
Ddit4	1.7510882	0.000376546	Increased
Brd2	1.29639	0.000378891	Increased
1200015M12Rik	1.593734	0.000392613	Increased
Hmgcs2	2.4088166	0.000411512	Increased
Rhob	1.3249034	0.000411894	Increased
Paxbp1	1.0157174	0.000415804	Increased
Csrp1	1.2047214	0.000428473	Increased
Klf11	1.3090526	0.000429472	Increased

(*Continues*)

Tables S1 Continued.

(*Continues*)

Tables S1 Continued.

Genes	logFC	FDR	Increased/ Decreased
Thbs1	1.7627576	0.000438951	Increased
Plat	1.0781324	0.000469502	Increased
Larp4	1.0081838	0.000474823	Increased
Angptl4	1.633707	0.000501922	Increased
Xrn2	1.0825716	0.000502888	Increased
Btg1	1.0037486	0.000518656	Increased
Dusp16	1.0504146	0.000525374	Increased
Gnl3	1.2077108	0.000530417	Increased
Ptpn12	1.1616296	0.000536581	Increased
Cyp4a10	1.0490442	0.000544744	Increased
Per1	1.466827	0.00055608	Increased
Apold1	1.5332164	0.000560097	Increased
Cyp4a14	2.620728	0.000570015	Increased
Tnfrsf12a	2.1595102	0.000621801	Increased
Akap12	1.7042044	0.000629186	Increased
BC027231	1.0250722	0.000660047	Increased
Rcan1	1.8326622	0.000701774	Increased
2410006H16Rik	1.5384626	0.000768415	Increased
Atf4	1.8051294	0.000783052	Increased
Atf3	3.1230954	0.000800625	Increased
Cyr61	2.256633	0.000814701	Increased
Maff	2.580911	0.000846273	Increased
Snhg5	1.1219932	0.00085587	Increased
Ier2	2.1315404	0.000880867	Increased
Aldh1a7	1.010667	0.000915946	Increased
Arpc1b	1.093803	0.000921596	Increased
Ifrd1	2.1264298	0.000933786	Increased
Adamts1	2.5678714	0.000952816	Increased
Cebpb	2.0909562	0.000954369	Increased
Inhbb	2.6247878	0.00095606	Increased
Btg2	2.6888518	0.000971343	Increased
Phip	1.3366428	0.001008023	Increased
Rasd1	1.4004466	0.001080442	Increased
Hoxd9	1.2812082	0.001099639	Increased
Suco	1.0709064	0.001123889	Increased
Ccnl1	1.102146	0.001137327	Increased
Zfp36	1.7037412	0.001152773	Increased
Dnajc7	1.0049556	0.001155786	Increased
Dusp5	1.7167594	0.001178172	Increased
Nab2	1.0497334	0.001267394	Increased
Smad1	1.0319196	0.001277789	Increased
Nbeal1	1.0334836	0.00129925	Increased
F2rl1	1.1391472	0.001455435	Increased
9930031P18Rik	1.470792	0.001491304	Increased
Slc20a1	1.3082052	0.001499575	Increased
Rora	1.106054	0.001556606	Increased
B230214O09Rik	1.1353122	0.001598764	Increased
Arg2	1.7022884	0.001609175	Increased
Chka	1.5028956	0.001641978	Increased
Cyp27b1	1.9070534	0.001764286	Increased
Klf6	2.657135	0.001789096	Increased

(*Continues*)

Tables S1 Continued.

Genes	logFC	FDR	Increased/ Decreased
Junb	2.4238854	0.001825288	Increased
Rela	1.0284526	0.001911428	Increased
Egr1	3.0782512	0.001967699	Increased
Zswim6	1.188642	0.002013913	Increased
Crim1	1.2947338	0.002096038	Increased
Aqp3	1.0719644	0.002179831	Increased
Brd4	1.283438	0.0022164	Increased
Bptf	1.1691922	0.002252835	Increased
Lgals3	1.1449486	0.002414167	Increased
Myc	2.480122	0.002443814	Increased
Irgm2	1.171169	0.002478475	Increased
Hbegf	2.2599608	0.002511907	Increased
AI314760	1.0038576	0.002629705	Increased
G0s2	1.256166	0.002677562	Increased
Pnrc1	1.3827078	0.002706595	Increased
Icam1	1.2722854	0.002822266	Increased
Thbd	1.1385316	0.002853051	Increased
Cldn4	1.2054326	0.002923268	Increased
Ccdc120	1.4132008	0.003066196	Increased
Itgav	1.076574	0.003087785	Increased
Gm19773	1.0925602	0.003127049	Increased
Fos	3.1534654	0.003280223	Increased
Pvr	1.7510692	0.00335116	Increased
Litaf	1.0853182	0.003372327	Increased
Bex1	1.1034186	0.0034641	Increased
Thrap3	1.0113736	0.003494435	Increased
Hmox1	2.063318	0.003528065	Increased
Crem	1.5370458	0.003541576	Increased
Gm3579	1.0411418	0.003591769	Increased
Snhg1	1.4227578	0.003771076	Increased
Prmt1	1.4056124	0.003850531	Increased
Adamts4	1.690825	0.003975197	Increased
Rnd3	1.5486354	0.004377426	Increased
Pmaip1	1.9273834	0.004671617	Increased
Taok1	1.0564312	0.004982616	Increased
AI503316	1.1067044	0.005080755	Increased
Nfkbiz	1.7581112	0.005119188	Increased
Dusp4	1.0591436	0.005253556	Increased
Ndfip2	1.4412588	0.005384564	Increased
Ptgs2	1.2432524	0.006559699	Increased
Lcn2	2.6595044	0.006875947	Increased
Gm13889	1.030244	0.006933953	Increased
Akt1s1	1.1719748	0.007121395	Increased
Pprc1	1.2706394	0.007164684	Increased
Baz1a	1.1241786	0.007478517	Increased
Sh3d19	1.0091054	0.007607386	Increased
5330406M23Rik	1.327714	0.008128809	Increased
Gm13363	1.3315994	0.009302486	Increased
AI845619	1.1630614	0.009626343	Increased

logFC: logarithmic fold change; FDR: false discovery rate (P-value adjusted for multiple tests).

Table S2 78 down-regulated genes identified in the mice with sepsis-induced multiple organ dysfunction syndrome (MODS) challenged by a combination of MV+SA through the GEO database.

Genes	logFC	FDR	Increased/ Decreased
Slc51a	-1.4491248	1.62E-08	Decreased
Nmrk1	-1.6789106	4.17E-08	Decreased
Mvd	-1.0804706	6.04E-08	Decreased
Marcks	-1.172523	3.15E-07	Decreased
Ldlr	-1.0914734	4.50E-07	Decreased
Afap1l1	-1.4388484	5.32E-07	Decreased
Trim63	-1.2807764	6.58E-07	Decreased
Col3a1	-1.3282152	9.05E-07	Decreased
Unkl	-1.0738096	1.05E-06	Decreased
Odc1	-1.4488874	1.54E-06	Decreased
Adamts5	-1.3067766	2.29E-06	Decreased
Fam69b	-1.004822	2.40E-06	Decreased
Cdh11	-1.646756	2.98E-06	Decreased
Zfp810	-1.0189208	2.99E-06	Decreased
Rbp1	-1.214556	3.00E-06	Decreased
Msmo1	-1.2658008	4.19E-06	Decreased
3110045C21Rik	-2.5692332	4.63E-06	Decreased
Col1a2	-1.4424306	5.14E-06	Decreased
Nxpe3	-1.194199	5.19E-06	Decreased
Dapk2	-1.1036162	5.31E-06	Decreased
2610528J11Rik	-1.0541544	5.92E-06	Decreased
0610005C13Rik	-1.1833912	6.27E-06	Decreased
Hpgd	-1.6374138	7.15E-06	Decreased
Vps8	-1.2304456	7.45E-06	Decreased
G6pc	-1.0782976	7.74E-06	Decreased
Ubiad1	-1.0369176	7.76E-06	Decreased
Cckar	-1.8822404	1.47E-05	Decreased
Cks2	-1.2827302	1.47E-05	Decreased
Pecr	-2.079669	1.57E-05	Decreased
Hsf2bp	-1.9302552	2.09E-05	Decreased
Bend5	-1.139385	2.35E-05	Decreased
Gmpr	-1.0197738	2.41E-05	Decreased
Myo5a	-1.1152384	5.16E-05	Decreased
Dleu7	-1.2230426	5.27E-05	Decreased
Tril	-1.3450622	7.38E-05	Decreased
Olfml1	-1.060529	7.54E-05	Decreased
Coa6	-1.2035438	8.58E-05	Decreased
Idi1	-1.7319858	9.34E-05	Decreased

(*Continues*)

Tables S2 Continued.

Genes	logFC	FDR	Increased/ Decreased
4-Sep	-1.078486	9.48E-05	Decreased
Slc46a3	-1.0572402	0.000105196	Decreased
Cdc42ep3	-1.0124138	0.000113824	Decreased
Ifi27l2a	-2.0243114	0.000165752	Decreased
Susd3	-1.0266302	0.000175497	Decreased
Slc7a13	-3.1806752	0.000188152	Decreased
Aacs	-1.4309022	0.000204064	Decreased
Hsd3b3	-1.0192154	0.000221846	Decreased
Fabp5	-1.1857218	0.000240987	Decreased
Cyp51	-1.0703666	0.000267356	Decreased
Car3	-1.4492312	0.000269619	Decreased
Lyrm2	-1.0627742	0.000312609	Decreased
Tmem25	-1.2281368	0.000379814	Decreased
Ube2u	-1.1370918	0.000413694	Decreased
Cenpj	-1.6242876	0.000421312	Decreased
Neu2	-1.0125656	0.000425471	Decreased
Pdp2	-1.0850616	0.00046105	Decreased
Mfsd2a	-1.8991474	0.000503334	Decreased
Sucnr1	-1.49824	0.000566494	Decreased
Cml1	-1.372691	0.000591407	Decreased
Eaf2	-1.267748	0.000621227	Decreased
D630023F18Rik	-1.4505818	0.001005148	Decreased
Bco2	-1.0205224	0.001205673	Decreased
Mrpl41	-1.0636954	0.001271703	Decreased
Mep1b	-1.00948	0.00128632	Decreased
Cela1	-1.0258084	0.001306119	Decreased
Fasn	-1.1051652	0.001353295	Decreased
Pycard	-1.0108376	0.00136777	Decreased
Amacr	-1.0071228	0.001816507	Decreased
D630024D03Rik	-1.0181288	0.002022474	Decreased
Thrsp	-1.7790314	0.002055292	Decreased
Med21	-1.1545338	0.002340529	Decreased
Tfec	-1.1726196	0.002392658	Decreased
Rpa3	-1.0741986	0.002539066	Decreased
Glyctk	-1.0188016	0.003235218	Decreased
Hsd3b2	-1.0027694	0.004173248	Decreased
Gm17750	-1.2178012	0.004852504	Decreased
Slc22a29	-1.0227594	0.00656575	Decreased
Adipoq	-1.589558	0.007925012	Decreased
D4Ertd298e	-1.1072004	0.009602492	Decreased

logFC: logarithmic fold change; FDR: false discovery rate (P-value adjusted for multiple tests).